

pubs.acs.org/JPCC Article

Nanosecond Diffuse Reflectance Spectroscopy for In-Situ Analysis of Electron Back-Recombination and Dye Regeneration in Fully Functional, Highly Efficient, Opaque Dye-Sensitized Solar Cell Devices

Elham Ghadiri* and Jacques-E. Moser



Cite This: J. Phys. Chem. C 2023, 127, 23285–23295



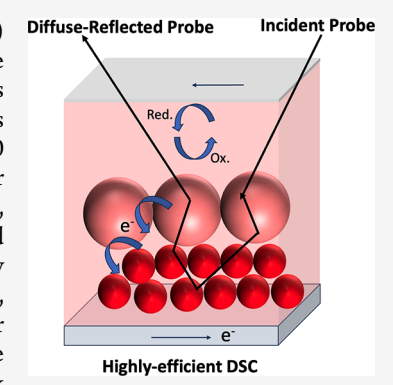
ACCESS I

Metrics & More

Article Recommendations

s) Supporting Information

ABSTRACT: An improved optical design for nanosecond diffuse reflectance (DR) spectroscopy is presented. The in-situ analysis of the electron back-reaction and dye regeneration processes in efficient opaque dye-sensitized solar cell devices (DSCs) was scrutinized for the first time using nanosecond DR spectroscopy. The efficient DSC device is based on an opaque TiO₂ double-layer film comprising 400 nm light-scattering particles and 20 nm optically transparent particles. Transmission-based laser techniques are not suitable for studying these or other devices by using the opaque morphologies of TiO₂ films. However, time-resolved DR flash photolysis enables the exploration of photophysical processes in a broad variety of opaque or highly light-absorbing and light-scattering materials. We experimentally verified the three important components of DR-based spectroscopy: optical configuration, sample condition, and theoretical quantitative optical models. The large optical angle for diffusive light enables efficient light collection and measurement at a relatively low power. We tested the steady-state and time-resolved concentration dependence of the Kubelka–Munk



theory for the quantitative analysis of time-resolved results and observed that the dynamics of electron back-reactions are strongly affected by the morphological parameters of the TiO_2 films. With a lifetime of 50 μ s, the kinetics of electron back-recombination in the device's photoanode, which is manufactured with 400 nm TiO_2 particles and 20 nm TiO_2 particles, are 2 orders of magnitude faster than what has been reported to date for 20 nm particles (1 ms). In contrast to electron back-recombination, the dye regeneration process is not influenced by the TiO_2 film morphology.

INTRODUCTION

The development of the laser flash photolysis technique by George Porter and Ronald Norrish in 1949 enabled the photochemical, photophysical, and photobiological analyses of short-lived photoinduced processes. 1-6 The flash photolysis technique uses an intense flash of light (the photolysis flash) that is usually provided by a xenon arc lamp to excite the sample to an intensity sufficient to produce a large population of intermediates (such as excited states, ions, radicals, and isomers); these can be detected by a second flash tube or lowrepetition laser with a nanosecond pulse width. As such, the technique allows for the study of photoinduced processes in the microsecond-to-millisecond time domain. Flash photolysis later evolved into pump-probe spectroscopy, which uses femtosecond laser pulses and advances electronic detection to push the time resolution limit to femtoseconds. However, in their conventional spectroscopy schemes, flash photolysis and pump-probe techniques are limited by the optical transparency of the samples because the detection of intermediate species is based on the transmission of the beam and measurement of the optical absorbance change. At the same time, many useful biological systems, materials, and devices are

opaque, highly light scattering, or highly light absorbing. Therefore, the propagation of light through such systems cannot be calculated using the Beer–Lambert law, as is conventionally performed in flash photolysis or pump–probe techniques. Frank Wilkinson and Rudolph Kessler developed a method for integrating diffuse reflected light with flash photolysis in the microsecond regime^{7,8} in 1981 and applied the technique to scattering systems like powders of organic microcrystals. When the irradiated light penetrates the sample, it is either absorbed or scattered; the re-emission of the scattering components from the irradiated side is deemed the diffuse reflected component. This diffuse reflection provides information from the bulk in contrast to specular reflection or a reflection from surface roughness. The interplay between absorption and scattering of components defines the amount

Received: August 9, 2023 Revised: October 31, 2023 Accepted: October 31, 2023 Published: November 20, 2023





of diffuse reflected light. The Kubelka-Munk theory associates the absorption and scattering intensities with the concentration, albeit within its own limitations.9 The irradiation, detection angle geometry, and optical elements associated with the collection of diffuse reflected light are of particular importance. In early works, Wilkinson et al. used an optical lens to collect only 3-4% of the diffuse reflected light from powders in the laser flash-photolysis scheme, wherein dramatically high excitation energies of 20 mJ/pulse (64 mJ/ cm²) were required to satisfactorily detect the transient species.^{7,8} They showed that the extremely high excitation powers caused interfering photothermal effects. To Using the same strategy for collecting diffuse reflection beams, the technique was used to study dye-modified light-scattering microcrystalline cellulose; however, extremely high excitation powers up to 2000 μ J focused on a small sample area of 0.14 cm² resulted in extremely high fluences of up to 14 mJ/cm².¹¹ Ghadiri et al. reported advanced optical probe using diffusereflectance based transient absorption spectroscopy and microscopy in femtosecond time domain for in-situ analysis of energy conversion and bioelectronic materials and devices.3

There is some ambiguity in the literature regarding photochemical studies using flash photolysis. In a study of TiO₂ (one of the most studied photocatalysts), Bahnemann et al. recently observed a color change from white to gray-blue after laser flash photolysis at high excitation powers (40 mJ/ cm²) in TiO₂ which remained for a very long time (several days and months). 12 Some groups attributed these variations to a change in crystalline phase from anatase to rutile. Bahnemann et al. determined that although using laser pulses of 40 mJ/cm² per pulse and temperatures up to 680 °C required for such a transition could occur, a thermal phasechange process was less probable because it contradicted the findings of Stopper and Dohrmann. 12,13 The latter showed (via time-resolved optoacoustic calorimetry) that 88% of the released heat is dissipated in a few nanoseconds over the system; thus, no significant temperature increase would be observed.¹³ Bahnemann et al. and others associated their observation with the nonthermal formation of long-lived trapped electrons and of Ti³⁺ by the laser; this is supported by electron paramagnetic resonance (EPR) studies as a plausible mechanism.

Despite the great potential of diffuse reflectance flash photolysis, there is little published literature on this topic owing to the aforementioned challenges; this underlines the need for a better optical probing method. In our current study, we showed that time-resolved diffuse reflectance-based laser flash photolysis studies are performed at much lower excitation regimes (few $\mu J/cm^2$) by improving the optical configuration of light collection as a nondestructive method. We also discuss the criteria and application of Kubelka–Munk model for quantitative data analysis.

Dye-sensitized solar cells (DSCs) are a promising alternative for cost-effective photovoltaics owing to their ease of fabrication with a relatively low cost, high efficiency under low-density illumination, and customizable aesthetics. ^{14–17} The performance of DSCs is based on a kinetic competition between an array of electron transfer processes in the absence of a built-in electric field to drive the charge separations. ⁴ These charge carrier processes include the injection of electrons from a sensitizer to the electron-collecting material (usually TiO₂), regeneration of the oxidized dye with a redox

electrolyte, and unwanted back-reactions of injected electrons recombining with oxidized dye molecules or oxidized species of redox electrolytes.4 Using femtosecond and nanosecond laser spectroscopy (absorption or emission spectroscopy; pump-probe terahertz), the kinetics of electron injection has been reported to be in femtoseconds-picoseconds while the electron back-recombination is in milliseconds. 4,18,19 The electron injection, back-recombination, and dye regeneration have been studied extensively using dye-sensitized transparent TiO₂ films on glass substrates or in solution; however, there have been no comprehensive analyses of the array of electron processes that occur in parallel by using a functional device. The main challenge is that such structures are mainly opaque or turbid, rendering the characterization of charge carriers using conventional optical transmission-based laser spectroscopy experiments impossible. A high-performance DSC device usually consists of a double-layer TiO2 film that contains a scattering layer comprising 400 nm TiO₂ particles deposited on top of a mesoporous transparent film. According to the Mie scattering theory, the light scattering efficiency is largely dependent on the size of the scattering particles as well as the wavelength of the incident light.²⁰ The theoretical scattering coefficient of a single TiO2 sphere in the ultraviolet-nearinfrared spectral range²¹ and the scattering parameters versus particle diameter for single TiO2 particles at various wavelengths²² for isotropic and anisotropic collective scattering in DSC electrodes²³ were calculated using the Mie theory. The 400 nm scattering particles are used in standard DSC photoanodes with the aim of improving the light-harvesting efficiency, specifically in the 600-700 nm wavelength region where the typical standard dyes show maximum optical absorption.²⁴ The presence of a scattering layer renders the photoanode optically opaque. We previously reported the electron injection dynamics in fully functional DSC devices based on the standard Ru-based (Z907) and organic D- π -A (Y123) dyes under in-operando conditions using femtosecond diffuse reflectance spectroscopy¹⁹ and showed an early recombination of photoinjected electrons in 20 ps after excitation in a complete device based on the Ru-based dye. Additionally, an intramolecular charge recombination in Y123 resulted in the lifetime photoinjection of 2 ps. 19 In this study, we explored the back-recombination process in complete DSC devices.

For nanosecond time-resolved DRTAS studies, using advanced optical configuration, we performed measurements at much lower excitation pulse energies free from artifacts and in the order of what is used in laser flash photolysis studies of transparent samples in transmission mode.² We also ascertained that the transmission and DR-based measurements were in agreement and also verified the photostability of the chromophores and reproducibility of the signal after several measurements. The integration of the Kubelka-Munk formalism for quantitative optical analysis of the steady-state and time-resolved diffuse reflectance measurements of opaque light scattering DSCs constructed with double-layer TiO2 films was also experimentally verified. Our data showed that the dynamics of charge carrier processes in a fully standard and efficient DSC device constructed of double-layer film and a standard Z907 Ru-based dye is markedly different than what has been reported in the literature for model dye-sensitized transparent films on glass or solution-phase measurements.

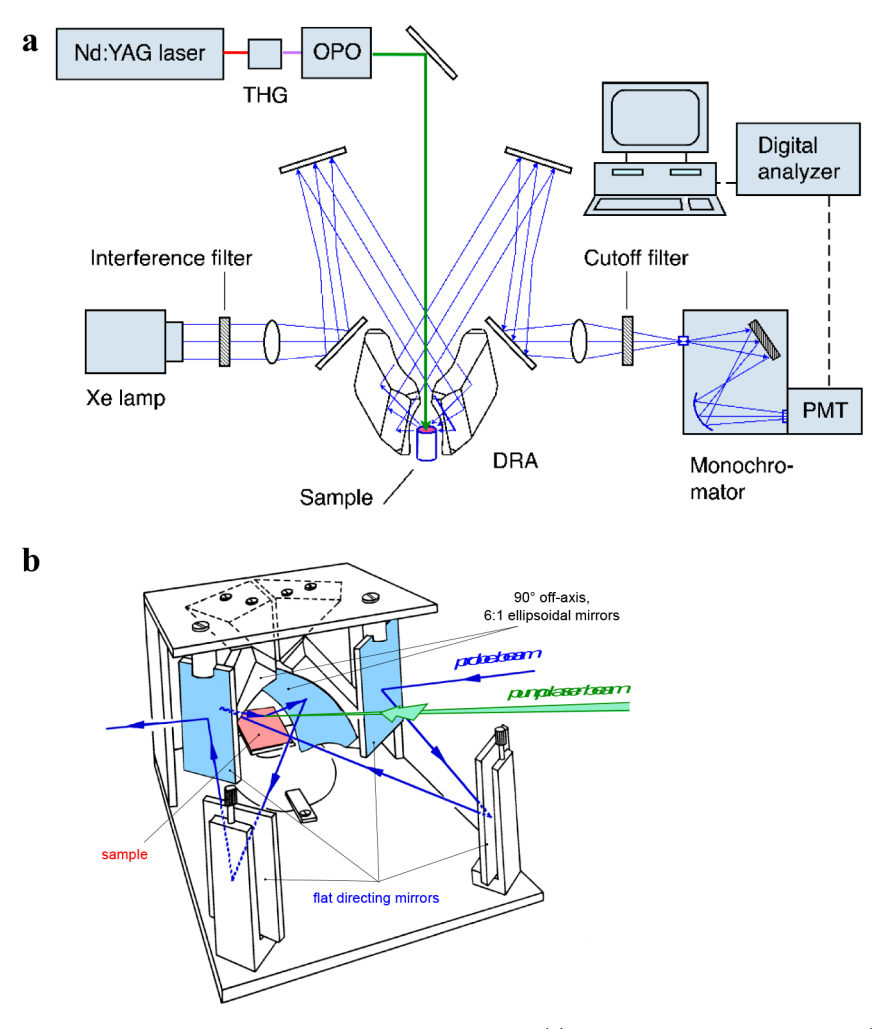


Figure 1. Scheme of the nanosecond transient diffuse reflectance spectrometer. (a) The pulsed excitation source (7 ns pulse length, 20 Hz repetition rate) is constituted by an optical parametric oscillator (OPO) pumped by a Q-switched frequency-tripled Nd:YAG laser. (b) Detailed sketch of the diffuse reflectance accessory (DRA). This optical configuration enables intercepting approximately 20% of the total reflection of opaque samples at all angles between 0° and 90°. The beam paths for excitation and light collection are shown. This setup allows performing measurements at much lower excitation pulse energies of $50-200 \ \mu J/cm^2$, which is comparable to the power used for the transmission-based technique.

■ EXPERIMENTAL METHODS

Nanosecond Diffuse Reflectance Flash Photolysis Spectroscopy. In principle, the configuration of nanosecond diffuse reflectance flash photolysis spectroscopy is similar to that of traditional transmission-based techniques. Short laser pump pulses excite the sample, while a continuous light source, such as a xenon lamp, probes the response. The differences are in the probe beam geometry that collects the diffuse reflected light, in the optical configuration of the sample, and in the optical model for data treatment.

In nanosecond diffuse reflectance flash photolysis (Figure 1), a pulsed excitation beam ($\lambda = 500-600$ nm, 5 ns FWHM pulse duration, $100~\mu\text{J/cm}^2$ pulse energy fluence, 30 Hz repetition rate) is provided by an optical parametric oscillator (OPO, GWU OPO-355) pumped by a frequency-tripled, Qswitched Nd:YAG laser (Continuum, Powerlite 7030). The excitation beam is passed through a plano-concave lens to irradiate a large cross section of the sample. The sample surface mounted on a modified Praying Mantis (Harrick) diffuse reflection accessory (Figure 1) has a 30° angle relative to the excitation beam. The probe beam is a continuous wave produced by a xenon arc lamp. The probe beam is passed

through a first tunable monochromator and is focused onto the sample using the first 6:1, 90° off-axis ellipsoidal mirror of the accessory. The diffuse reflected beam is collected by the second ellipsoidal mirror of the accessory, intercepting approximately 20% of the total reflection at all angles between 0° and 90° from the surface. The collected light is directed to cutoff filters and to a second monochromator before being detected by a fast photomultiplier tube and a DSA 602A digital signal analyzer (Tektronix). Averaging the signal over 2500 laser shots is necessary to obtain a satisfactory signal-to-noise ratio. The intensity of the probe at the detector with and without pump excitation is also recorded as R and R_0 , respectively, to be used for further analysis. This setup allows performing measurements at low excitation pulse energies of $50-200 \mu J/cm^2$, which is comparable to the power used in the transmission-based technique. In this study, transmissionbased experiments were performed as control tests using the same setup except that the DR accessory was removed, the sample was mounted on a solid sample holder, and the probe transmission was measured.

DSC Device and Photoanode. The structures and images of the three photoanodes constructed using different sizes of

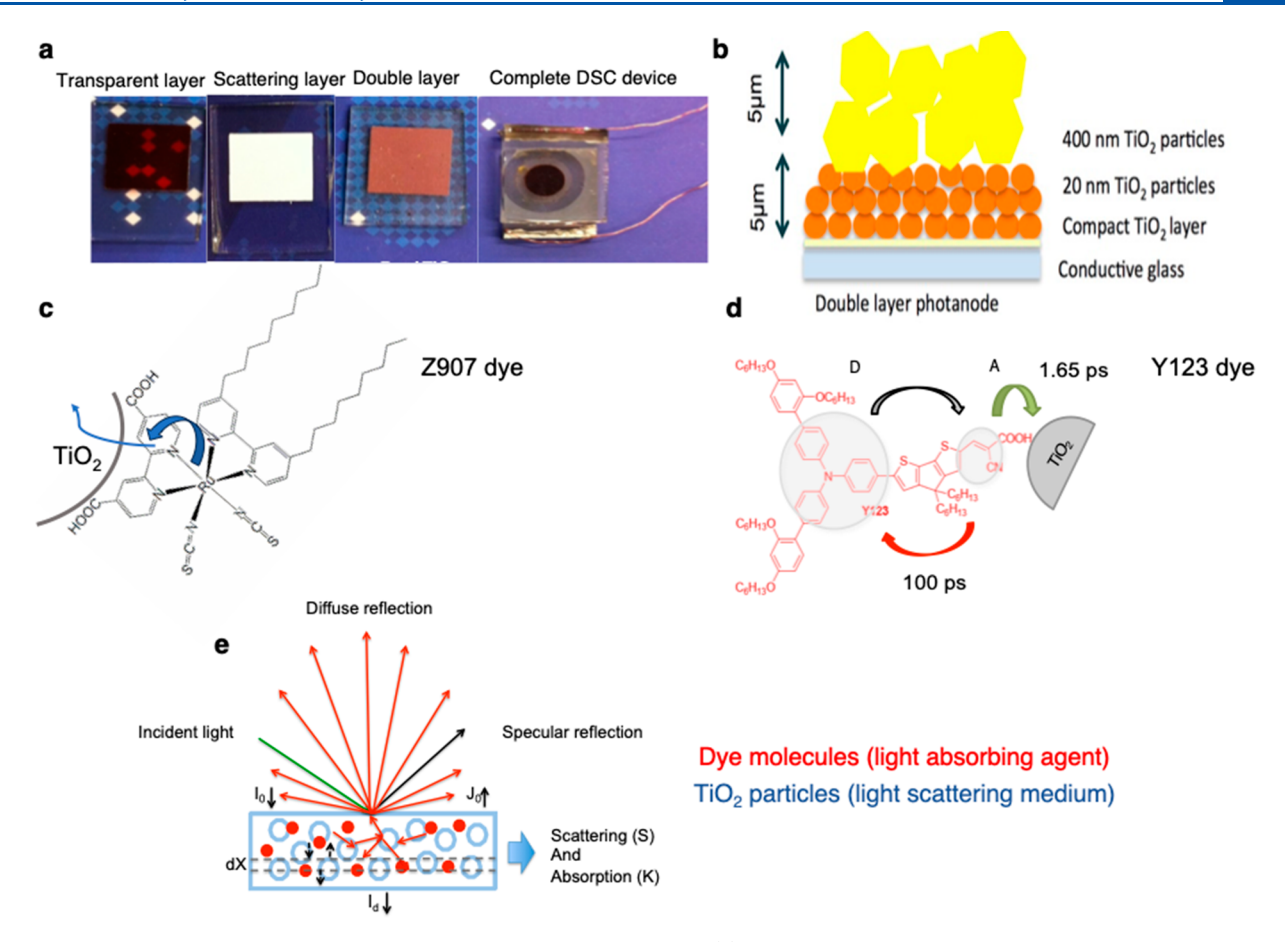


Figure 2. Structure of DSC photoanodes and liquid-electrolyte DSC device. (a) Photographs of the dye-loaded transparent TiO₂ film, TiO₂ double-layer photoanode, dye-loaded TiO₂ double layer, and fully functional encapsulated DSC. (b) TiO₂ double-layer structure used in highly efficient DSCs. (c) Molecular structure of the Z907 dye. (d) Molecular structure of the Y123 dye. The arrows indicate the ultrafast electron transfer steps after photoexcitation. (e) Schematic representation of the diffuse reflectance from optically opaque thick films constructed from scattering medium (TiO₂) and light absorbing components (dye molecules) on which the simplified Kubelka–Munk formalism is applied. Specular reflection (if present) is eliminated during measurements.

Table 1. Structure and Morphological Parameters of the Transparent TiO₂ Film-, Scattering TiO₂ Film-, and Double-Layer TiO₂ Film-Based DSC Photoanode^a

sample	TiO ₂ particles size (nm)	film thickness (μm)	porosity (%)	BET surface area (m² g ⁻¹)	roughness factor (cm $^2 \mu m^{-1}$)
transparent layer	20 ± 5	5 ± 0.5	70	85	98
scattering layer	400 ± 10	5 ± 0.5	65	27	36
double layer	20 + 400	$5 + 5 (\pm 0.5)$			

^aThe scattering layer contains a small fraction of 10 nm particles. The structure of the photoanode is the same as that used when constructing standard efficient DSC devices; this includes the compact TiO₂ underlayer and TiO₂ prepared by surface treatment (see the Experimental Methods section).

TiO₂ particles that were prepared using the screen-printing method are depicted in Figure 2a and Table 1. The procedure for creating these films was identical to the standard method used for the fabrication of highly efficient DSC devices. Prior to film deposition, a TiO₂ underlayer was deposited on a precleaned conductive glass substrate (fluorine-doped tin oxide-coated glasses, TEC15, Solaronix), using a TiCl₄ solution (40 mM) at 80 °C. A 5 μ m thick layer of 20 nm particles was screen-printed onto the substrate to create a transparent layer. To prepare the standard double-layer film (Figure 2b), another 5 μ m thick layer of scattering particles (400 nm diameter) was screen-printed on top of the transparent layer. For the preparation of the scattering paste, 10 nm TiO₂ particles were mixed with 400 nm particles with a final paste formulation of 2.9% 10 nm TiO₂, 28.6% 400 nm

 ${
m TiO}_2$, and 7.2% ethyl cellulose in terpineol. The printed surface area in all films was 1 cm². The films were then sintered following a series of firing steps (325 °C for 5 min with a 15 min ramp time, 375 °C for 5 min with a 5 min ramp time, 450 °C for 15 min with a 5 min ramp time, and 500 °C for 15 min with a 5 min ramp time, and 500 °C for 15 min with a 5 min ramp time) to remove the polymeric binders and ensure better electronic contact between particles. The thicknesses of screen-printed films were measured by using a KLA Tensor Alpha-Step 500 profilometer. Another ${
m TiCl}_4$ treatment was applied to the films. Prior to dye loading, photoanodes were sintered again at 480 °C for 30 min. Finally, the films were cooled to 80 °C and immersed in the dye solutions overnight at room temperature.

Prior to performing the experiments, samples are dipped and washed in acetonitrile for approximately 1 h. For device

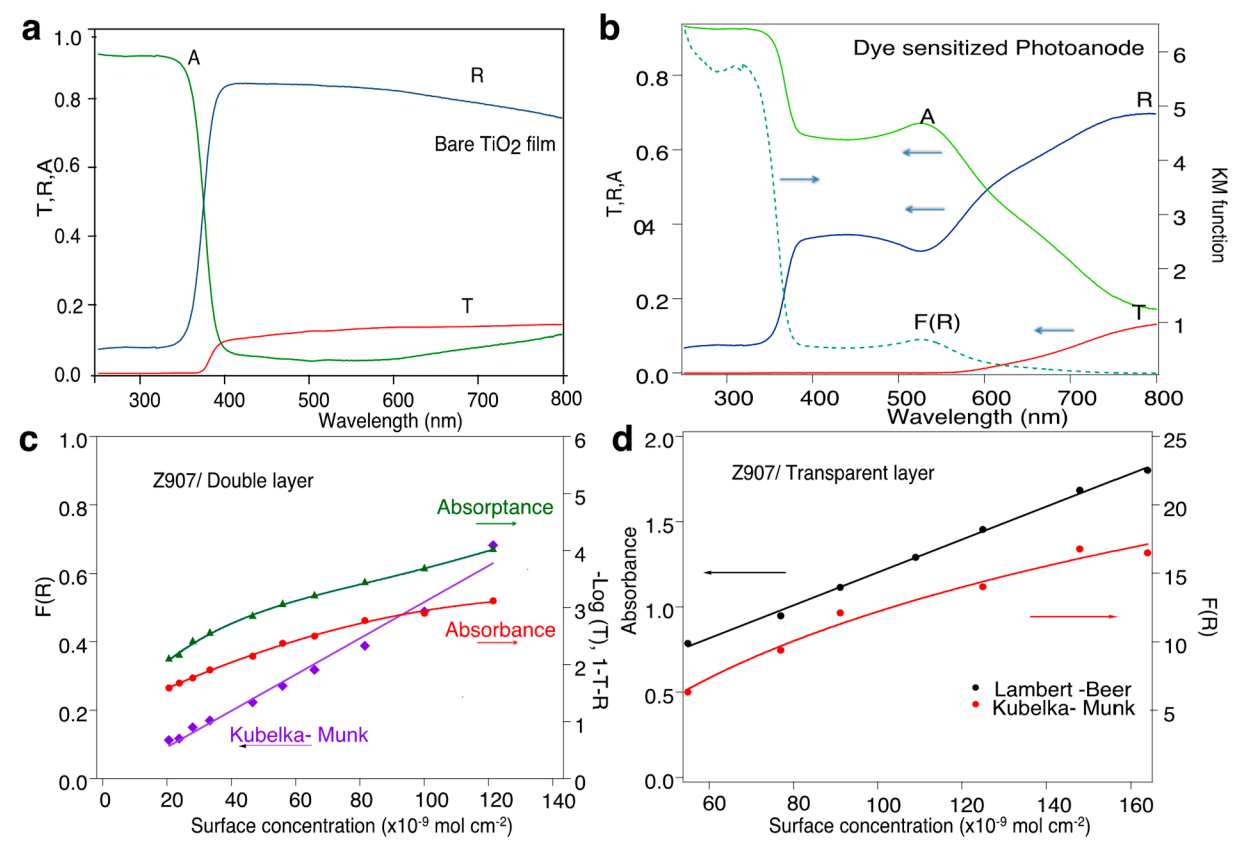


Figure 3. Experimental verification of optical theories on DSC photoanodes. Total transmittance (red), diffuse reflectance (blue), absorptance (green), and Kubelka—Munk function (dashed green) of (a) a bare standard TiO_2 film applied in high-performance DSCs and (b) a Z907-sensitized TiO_2 double-layer-based DSC photoanode. (c) Dye concentration dependence of the Kubelka—Munk function F(R) (left axis, purple diamond), absorbance ($-\log T$), and absorptance (1-T-R) (right axis, red and green, respectively) of a dye-sensitized double-layer film measured at 520 nm. While the Kubelka—Munk function almost shows a linear trend on the surface concentration of the dye, the other two functions, absorbance and absorptance, do not depict a linear trend. (d) Dye concentration dependence of the Kubelka—Munk function and absorbance for transparent dye-sensitized film. F(R) function does not show a linear relationship to the dye concentration in this case, and absorbance is the correct parameter for quantitative analysis.

fabrication, the dye-anchored substrates were rinsed with acetonitrile and sealed with pieces of thermally platinized counter electrodes that were created using a solution of H₂PtCl₆ on FTO glass (TEC15, Pilkington). The working and counter electrodes were separated by a 25 µm thick hot melt ring (Surlyn, DuPont) and sealed by heating. The electrolytes were then introduced to the cells via predrilled holes in the counter electrodes. In DSC devices, Z907 dye (Figure 2c) is used as the sensitizer with standard low-volatility iodide-based redox electrolytes (Z946). The Z907 dye is a standard and widely used Ru-based dye for efficient and stable DSC devices. Z907 dye (0.3 mmol concentration) is dissolved in a tertbutanol/acetonitrile solvent mixture (1:1 v/v). The iodidebased electrolyte coded Z946 is an I₃-/I⁻-based electrolyte in 3-methoxypropionitrile solvent. A typical I-V curve for the standard Ru-based Z907 dye and Z946 redox electrolyte is provided in Figure S1.

Our results are the summary of several measurements over Ru-based standard devices and organic sensitizers. Comparative studies were performed using Y123 (3-{6-{4-[bis(2',4'-dihexyloxybiphenyl-4-yl)amino]phenyl}-4,4-dihexylocyclopenta-[2,1-b:3,4-b]dithiphene-2-yl}-2-cyanoacrylic acid) (Figure 2d) as well as another Ru-based dye C101 ([NaRu(4,4'-bis(5-hexylthiophene-2-yl)-2,2'-bipyridine)(4-carboxylic acid-4'-carboxylate-2,2'-bipyridine) (NCS)2]) that has a higher light absorption than Z907. Y123 is an efficient organic dye with a

donor- π -acceptor (D- π -A) push—pull structure that has been found to be efficient when combined with Co-based electrolytes. D- π -A organic dyes are also used as nonfullerene electron acceptors in organic solar cells. The photograph and schematic of the DSC device are shown in Figure 2. We previously reported the dynamics of electron injection for both Z907 and Y123 dye-based devices using femtosecond diffuse reflectance transient absorption spectroscopy under in-operando conditions. In this study, we investigated the dynamics of back recombination and dye regeneration in DSC devices occurring over longer time scales in fully functional devices.

RESULTS AND DISCUSSION

Phenomenological Optical Theories. The Beer-Lambert law cannot be applied to diffuse reflectance spectroscopy of light scattering materials. This law states that there is a logarithmic dependence between the transmission (or transmittivity) of light through a substance and the product of the absorption coefficient of that substance on one hand and the distance that light travels through the material (the path length) on the other. This theory assumes that the absorbing medium does not scatter the light (i.e., no turbidity exists); however, this is not the case for opaque materials.

In the configuration of reflectance measurements, the transient absorptance change can be measured by determining the amount of diffuse reflected light with and without the pump beam. Therefore, the absorptance is displayed as:

$$\mathcal{A} = 1 - T - R \tag{1}$$

For opaque samples, the optical transmittance is negligible; the absorptance change (ΔA) can be deduced only from reflectance change as follows:

$$\Delta \mathcal{H} = 1 - \frac{R}{R_0} = 1 - \frac{\Delta R + R_0}{R_0} \tag{2}$$

where T is the intensity of the transmitted light and R and R_0 represent the intensity of the diffuse reflectance of the probe pulse with and without excitation, respectively.

The first attempt to provide a simplified solution for the radiation transfer equation in the simplest form for isotropic scattering was performed by Schuster, who provided the reflectance function assuming two oppositely directed radiation fluxes normal to the surface of the sample.^{28,5} Another theory widely used to describe the optical behavior of a tightly packed isotropic absorbing and scattering medium is the Kubelka-Munk theory, which uses the same differential equations and assumption as Schuster. The Kubelka-Munk function relates the measurable diffuse reflectance of the sample to the ratio of the absorption coefficient (k) and scattering coefficient (s). In diffuse reflectance measurements, Kubelka-Munk theory is generally used for the analysis of diffuse reflectance spectra obtained from weakly absorbing samples. It provides a correlation between reflectance and the concentration of the absorbing species and makes simplifying assumptions to accommodate Lambert's Cosine law. It applies to systems in which the scattering species is isotropically distributed (Figure 2e) and the specular reflection is ignored. The theory works best for optically thick materials that are sufficiently pigmented and wherein the particles constituting the layer are much smaller than the total thickness, the transmittance of the film is negligible, and the sample is subject to diffuse irradiation. The general hyperbolic Kubelka formulation is used in its simplified form, $F(R_{\infty})$ (eq 3), where R_{∞} represents the diffuse reflectance from the sample. For low concentrations c (i.e., a diluted absorber), the absorption coefficient k should be proportional to the concentration and the molar extinction coefficient of the absorbing medium in the same way as the Beer-Lambert law is valid in diluted medium. Therefore, the simplified Kubelka-Munk function is related to the concentration of absorbing species as shown in eq 3.9

$$F(R_{\infty}) = \frac{k}{s} = \frac{(1 - R_{\infty})^2}{2R_{\infty}} = \varepsilon c \frac{\ln(10)}{s}$$
(3)

Experimental Verification of the Simplified Schuster–Kubelka–Munk Theory. The total transmittance through the bare TiO_2 double-layer film was less than 15% (Figure 3a). The films were opaque, and the surface is matt as Figure 2a shows; hence, the diffuse reflectance is the dominant process, and the specular reflectance is negligible. Under such conditions, diffuse reflectance appears to be the only technique to study the charge carriers' kinetics within a device created with such opaque films. The total transmittance, reflectance, and absorptance together with the $F(R_{\infty})$ function spectrum of the Z907 dye-sensitized TiO_2 double layer are shown in Figure

3b. Approximately 70% of the light is absorbed in the bluegreen region. The Kubelka-Munk spectrum follows the shape of the absorptance with a peak at 520 nm (characteristic of the absorption of the Z907 dye) and a shoulder at 380 nm due to the absorption of TiO2. In the DSC photoanode, one monolayer of dye is ideally adsorbed on the surface of the mesoporous film with a high roughness factor (approximately 1000 for a 10 μ m film) (diluted system) and TiO₂ particle sizes of 20 and 400 nm (much smaller than the total film thickness). Given these conditions of a diluted thick medium, the Kubelka-Munk theory can be applied for the quantitative analysis of reflectance and determining the concentration of absorbing species with good approximation. The evolution of the Kubelka-Munk function upon dye concentration change for TiO2 double-layer-based photoanode at different wavelengths is provided in Figure S2. For transparent-based photoanodes, the evolution of absorbance spectrum upon concentration dye concentration variation is shown in Figure

The validity of Kubelka-Munk theory for the quantitative optical analysis of standard liquid cell DSC devices was experimentally tested. The concentration of Z907 dye adsorbed in the film gradually decreased, owing to partial desorption of dye molecules. The desorbing solution had to allow for gradual desorption of Z907 within a practical experimental time scale. A solution of 0.1 M NaOH in MeOH:H₂O (1:1) was first tested. While desorption was indeed observed after a few hours, the process was practically too slow. A solution of 0.05 M DMF:TBAOH was tested. The desorbing process was faster and compatible with experimental protocol (Figure S4). The optical response of the film (i.e., diffuse/total transmittance and reflectance) at each concentration was measured. Three different optical formalisms were applied to the optical response of the films at 520 nm as a function of dye surface concentration; the results for doublelayer film were compared (Figure 3c). For the double-layer film, the Kubelka-Munk function showed a good linear trend over the concentration of the absorber; however, the absorbance and absorptance curves of the film did not show such a linear trend. In previous studies performed on coumarin dye-sensitized TiO2 film with a fractal structure, the absorptance of the sample was shown to be linearly dependent on the dye concentration only if the surface coverage was less than 0.2 or yielding an absorptance less than 40%. For the transparent film, the absorbance $(-\log(T))$ shows a linear correlation with the concentration of the dye on the film (as expected). Given the above, the KM function was applied for quantitative analysis of transient spectroscopy of opaque samples, and the Lambert-Beer law was used for transparent films.

Error analysis was performed for steady-state optical measurements. For measurements with an integrating sphere, one issue was that the sizes of its entry and exit holes were relatively large compared to its internal surface area. Two cardboard masks were placed directly on the outer surface of the integrating sphere. The mask itself is not 100% reflective, but because the baseline correction is performed with the mask in place, a comparison of all samples should be feasible. For defining the dye surface coverage, in practice, a 100% dye desorption could not be attained (as Figure S2 shows); the samples remained palely colored. This was most pronounced for the double-layer film with the highest expected surface area (and therefore loaded dye), less so for the transparent and

scattering film. While this undermined the absolute value of the dye surface concentration determined, it is not expected to affect the trend of the optical characteristics of the samples (KM, absorbance, absorptance) versus dye surface coverage. The dye was gradually desorbed by consecutively dipping the sample into the same solution. A solution loss inevitably resulted from taking the samples in and out of the desorbing solution. While this affected the accuracy of the concentration determination, this error was of the same order of magnitude for all three samples (concentrations should not be considered as absolute values; they should allow comparison of the three systems).

In-Situ Analysis of Electron Back-Recombination in Device. We performed an in-situ analysis of the dynamics of electron back-recombination from TiO₂ with the oxidized dye molecules; moreover, the dye regeneration process in the complete DSC device was investigated using nanosecond time-resolved diffuse reflectance spectroscopy measurements. Equations 4 and 5 represent the electron back-recombination and dye regeneration processes with a redox mediator, respectively:

$$e_{cb}^{-} + S^{+} \to S \tag{4}$$

$$S^+ + Re \rightarrow S + Re^+ \tag{5}$$

where S stands for sensitizer and Re stands for reducing agent. The oxidation state of the Z907 dye adsorbed on the opaque TiO₂ film was monitored at 650 nm, which is the characteristic wavelength of the Z907 oxidized dye's absorption. For transparent film and scattering layer based photoanodes, mostly front-side irradiation (TiO₂ side) is used. For the double-layer photoanode sample, back-side irradiation (conductive glass side) is used to ensure light can reach both transparent and scattering layers. For a complete device that includes Pt-based photocathode as well (the right image in Figure 2a), the back-side illumination (from anode conductive glass side) is indispensable. In all half-cell measurements above, films are covered with a thin layer of redox-inactive solvent (or redox-active electrolyte) topped with a cover glass to protect the sample during measurements.

In the absence of a redox electrolyte, the decay kinetics (depicted in Figure 4) reflects the dynamic of the backreaction of electrons with oxidized dye molecules. The kinetics of electron back-recombination were compared when the dye was adsorbed on three different TiO2 electrodes: a transparent layer, scattering layer, and double layer. All three samples were measured by using the nanosecond diffuse reflectance technique. The silver trace corresponded to the absorbance change of the Z907 oxidized dye when attached to 20 nm particles. The signal decayed with a half reaction time $(t_{1/2})$ of 1.0 ± 0.3 ms. Data fitted by a single exponential yielded a rate constant of $(6.8 \pm 1.6) \times 10^2$ s⁻¹. Our observed kinetics of the electron back-recombination in the dye-sensitized transparent film as measured using the diffuse reflectance method was consistent with those previously reported on transparent films measured using transmission-based techniques;⁴ this was expected as the measurement technique should not influence the result. The blue trace shows a transient decay of $F(\Delta R_{\infty})$ for S⁺ on scattering TiO₂ particles. Surprisingly, the halfreaction time $t_{1/2}$ for this sample was 70 \pm 4.0 μ s. The rate constant extracted by fitting with a single exponential is $1.3 \times$ $10^4 \pm 0.7 \times 10^3 \text{ s}^{-1}$. For the double-layer film, the decay of the oxidized dye signal was still accelerated, and the half-reaction

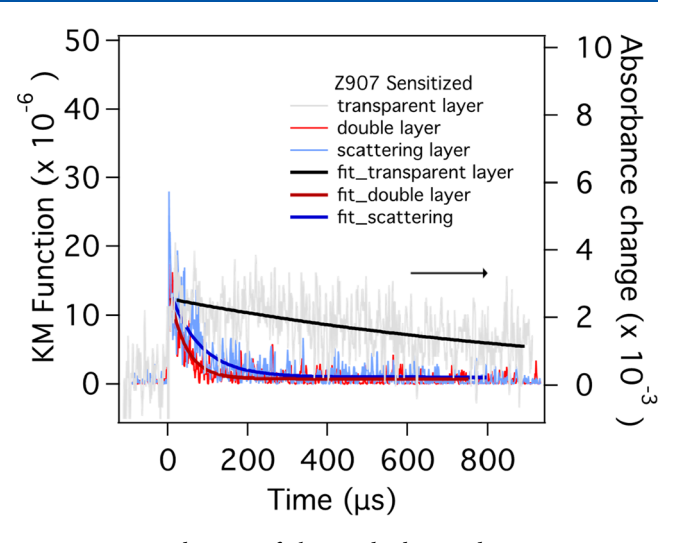


Figure 4. In-situ kinetics of electron back-recombination process in standard highly efficient DSC devices. Nanosecond diffuse reflectance measurements on a Z907 dye-sensitized photoanode recorded at 650 nm, which is relevant to dye oxidized state absorption. Shown are the red trace (double layer), blue trace (scattering layer), and black trace (transparent layer) in the presence of the redox-inactive solvent methoxypropionitrile. The KM function on the left was used for the opaque samples, while the absorbance formulation on the right was used for the transparent samples. Solid lines are fit to a single-exponential function.

time decreased to $38 \pm 2.0~\mu s$. The parameters of exponential fit function including the amplitude, rate, and uncertainty considering one standard deviation, as well as the fit residual trace, are provided in Figure S5 for all studied samples.

The decay of the oxidized dye's absorption on the scattering particles, and consequently in the double layer, was significantly accelerated by 2 orders of magnitude compared to transparent small particles. The silver trace appeared to be noisier than the other two because it was indeed a diffuse reflectance measurement on a transparent nonscattering film under very low pulse light excitation.

Notably, we applied the lowest possible pulse energies when investigating the electron back-recombination of photoinjected electrons with the oxidized dye. The low irradiance was to ensure that the reaction followed a first-order regime. Typically, one electron was injected per each 20 nm TiO₂ particle; therefore, the small absorption changes are due to this low excitation energy. A typical intensity-dependence measurement on a Z907-transparent photoanode comprising 20 nm particles while in transmission mode is shown in Figure S6. The excitation and probe wavelengths were 530 nm and 710 nm, respectively, and the excitation pulse intensity increased from 75 μ J to 300 μ J. At lower excitations of 75 μ J and 120 μ J, the kinetics were fitted with a single-exponential function with rate constants $k_1 = 1.1 \times 10^3 \pm 2.0 \times 10^2 \text{ s}^{-1}$ and $k_1 = 1.9 \times 10^3 \text{ s}^{-1}$ $10^3 \pm 2.4 \times 10^2 \text{ s}^{-1}$, respectively, giving a lifetime of approximately 1 ms for the back-recombination process. At a high excitation energy (i.e., 300 μ J), the kinetics were fitted with a double-exponential decay function with rate constants $k_1 = 2.2 \times 10^3 \pm 1.4 \times 10^2 \text{ s}^{-1} \text{ and } k_2 = 2.4 \times 10^4 \pm 1.3 \times 10^3$ s⁻¹. An example of an intensity-dependent measurement on an opaque double-layer photoanode is shown in Figure S7. By increasing the intensity, the amplitude of the signal and the signal-to-noise ratio increased. The kinetics were fitted with a single-exponential decay function at a lower excitation (95 and

119 μ J) and with a double-exponential decay fitting function at a higher excitation (300 μ J). As shown in Figure S8, the amplitude of the transient Kubelka–Munk function, and consequently the concentration of transient species, (oxidized dye, S⁺), shows a linear relation with the excitation power.

In our control tests, the kinetics of electron back-recombination in a transparent anode made of 20 nm particles is measured using either diffuse reflectance or in transmission mode (Figure S9) and the results agree with each other; the signal is fitted with an exponential decay function with a rate of $5.2 \times 10^3 \pm 2.7 \times 10^2 \ \text{s}^{-1}$ and $5.1 \times 10^3 \pm 2.8 \times 10^2 \ \text{s}^{-1}$, respectively. The results are consistent with the back-recombination lifetime values when using Ru-based dyes in sensitized transparent TiO_2 films constructed from 20 nm small particles on glass substrates as reported in the literature over several years. ^{2,4}

The in-situ analysis of the electron back-recombination process in efficient opaque DSCs made of a double-layer film using diffuse reflectance spectroscopy indicated that this process occurred over a time scale of microseconds, which is 2 orders of magnitude faster than what has been reported for transparent model systems^{2,4} constructed from 20 nm TiO₂ particles on glass.

In-Situ Analysis of Dye Regeneration in Devices. Figure 5 illustrates the dye regeneration process as investigated using DSCs constructed with transparent, scattering layer opaque, and double-layer opaque anodes in the presence of the standard iodide-based redox electrolyte Z946. All samples were measured in diffuse-reflectance mode. The decay kinetics

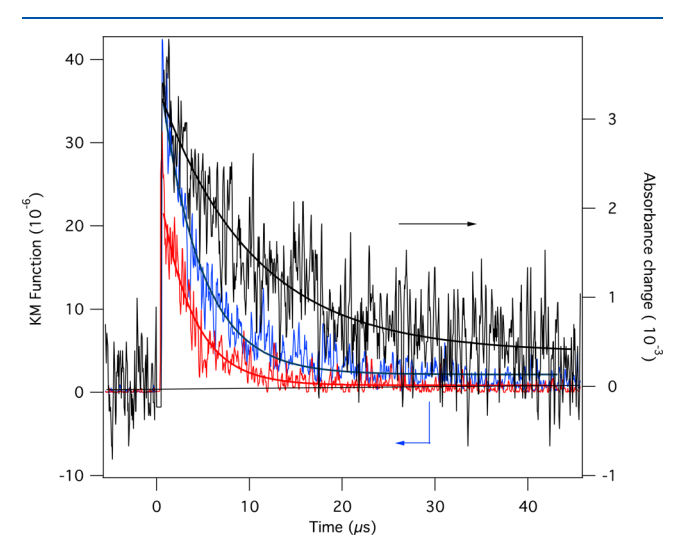


Figure 5. In-situ kinetics of dye regeneration process in standard highly efficient DSC devices. Nanosecond diffuse reflectance measurements of a Z907-sensitized DSC photoanode in the presence of a redox electrolyte. Shown are the red trace (double layer), blue trace (scattering layer), and black trace (transparent layer) in the presence of iodide-based electrolyte Z946. The Kubelka–Munk function F(R) is used for the transient diffuse reflectance for opaque samples, while the absorbance change is used for the transparent film. Solid lines indicate single-exponential decay functions fit to the results. The solid lines show the exponential fit of the data; the first-order rate constants were $k_1 = 9.8 \times 10^4 \pm 4.5 \times 10^3 \text{ s}^{-1}$, $k_1 = 2.3 \times 10^5 \pm 4.6 \times 10^3 \text{ s}^{-1}$, and $k_1 = 2.8 \times 10^5 \pm 6.8 \times 10^3 \text{ s}^{-1}$ for the transparent, scattering, and double-layer films, respectively. The kinetics of dye regeneration have the same orders of magnitude. While the rates are slightly different, they are not substantially changed (in contrast to the electron back-recombination process).

represents the reduction of the oxidized dye molecule by the redox electrolyte eq 5. The solid lines show the exponential fit of the data; the first-order rate constants were $k_1 = 9.8 \times 10^4 \pm$ $4.5 \times 10^{3} \text{ s}^{-1}$, $k_1 = 2.3 \times 10^{5} \pm 4.6 \times 10^{3} \text{ s}^{-1}$, and $k_1 = 2.8 \times 10^{5} \pm 4.6 \times 10^{3} \text{ s}^{-1}$ $10^5 \pm 6.8 \times 10^3 \,\mathrm{s}^{-1}$ for the transparent, scattering, and doublelayer films, respectively. Contrary to the electron back-transfer process, we observed that the dye regeneration rates were very similar across all three anodes in this case. The slight variation can be understood as the difference in the diffusion of redox species within the holes of the mesoporous transparent TiO2 as well as the TiO2 scattering layer or double-layer films, which can slightly affect the interception effectiveness. Based on this result, we conclude that the dye regeneration process is not influenced by the morphology of the TiO2 substrate. This result was foreseen given that this process is presumed to be more dependent on the redox potential of the dye's oxidized state and the electrolyte redox potential, which control the driving force of electron transfer during the dye regeneration process.

Dynamics of Photocarriers in a Complete DSC Device. The lifetimes of the electron back-recombination and dye regeneration processes extracted from nanosecond-diffuse reflectance spectroscopy measurements are shown in Table 2.

Table 2. Comparison of the Lifetimes of the Electron Back-Reaction versus Dye Regeneration Processes Occurring in DSCs Based on a Complete Double Layer, Scattering Layer, or Transparent Layer Anode Extracted from Nanosecond Diffuse Reflectance Measurements^a

	sample	$t_{1/2}(\mu s)$
in the presence of methoxypropionitrile solvent	transparent layer	1000 ± 200
	scattering layer	70 ± 4
	double layer	38 ± 2
device (in the presence of electrolyte)	transparent layer	10.0 ± 0.4
	scattering layer	4.3 ± 0.1
	full device (double layer)	3.6 ± 0.1

^aThe error is calculated based on one standard deviation of the fitting parameters of the exponential functions to results presented in Figures 4 and 5.

The dye regeneration yield was determined from eq 6

$$\eta_{\rm reg} = \frac{k_{\rm r}}{k_{\rm r} + k_{\rm b}} \tag{6}$$

where $k_{\rm r}$ is the first-order rate constant of the dye interception process by redox electrolyte (Re⁺/Re) in eq 5 and $k_{\rm b}$ is the rate constant of the recombination reaction in eq 4 that occurs between the oxidized state of the dye (S⁺) and electrons injected into the conduction band. The dye regeneration yield in a DSC based on a transparent TiO₂ film was 99%, while that in a double-layer complete device was found to be 93%.

Effect of Nanostructured TiO₂ Film Morphology. Our broader studies demonstrated that the morphology of ${\rm TiO_2}$ strongly affects the kinetics of back-recombination. Various ${\rm TiO_2}$ nanostructures (nanostructured fibers, nanosheets, nanotubes, nanorods, and scattering particles) are incorporated into different types of DSCs (solid state or liquid electrolyte devices), and their performances have been mainly characterized by routine photoelectrochemical and photovoltaic test

methods. Transient spectroscopy methods are widely used to study electron injection, dye regeneration, and back-recombination processes within—or at the interface of—transparent ${\rm TiO_2}$ films, dyes, and electrolytes. However, there are no published studies of any of the other ${\rm TiO_2}$ morphologies using optical pump—probe methods, as these nanostructures are often optically opaque. We were able to overcome this limitation using nanosecond diffuse reflectance spectroscopy.

In our previous studies of C101 dye-sensitized nanostructured fibers and QD-sensitized nanostructured fibers, enhanced DSC device performance³⁰ and enhanced photocatalytic characteristics³¹ were reported. We found that the electron back-recombination was even faster and in the microsecond range for fibers compared to small 20 nm particles; the half reaction lifetime was measured at 18 μ s on TiO₂ nanostructured fibers.³⁰ Using transient photovoltage/ photocurrent techniques, we found that the electron transport was faster in fibers than in 20 nm spherical particles.³⁰

Using diffuse reflectance flash photolysis, we also compared the electron back-transfer in Ru-based C101 dye-sensitized TiO₂ nanosheets and C101 dye-sensitized TiO₂ nanoparticles.³² The kinetics of the electron back-reaction process was again observed to depend on the morphology of the TiO2 film, and the it was 6-fold slower for dye-sensitized (001) TiO₂ nanosheets compared to dye-sensitized (101) TiO₂ nanoparticles.³² One possible explanation for the variation in the electron back-transfer kinetics could be the difference in the dye anchoring geometry in these two films. If we assume a damping coefficient $\beta = 1.2 \text{ Å}^{-1}$ for the through-space tunneling of electrons (eq 7), retardation of the charge recombination reaction by a factor of 6 corresponds to the increase of the electron transfer distance existing between the Ru(III) center of the oxidized dye and the closest Ti(IV) site on the surface of the oxide by $\Delta r = 1.5 \text{ Å}$.

$$k_{\rm b} = k_{\rm b}^0 \exp(-\beta \Delta r) \tag{7}$$

Different anchoring geometries are expected on the (101) crystalline and (001) crystalline surfaces.³² The distance between the Ru center of the dye and the Ti4+ ion directly linked to one of the oxygen atoms of the carboxylic anchor is approximately about 10 Å when the bpy adopts a flat structure. A change of the tilt angle of the bipyridyl rings related to the surface normal of ca. 15° on the (001) facet to ca. 35° on the (101) facet would yield a decrease of the distance between the Ru center in the dye to the surface of ~1.5 Å. It is worth mentioning that other than the geometrical distance between the oxidized dye molecule and the photoinjected electrons, the energetics of the TiO2 film can also play a role in the observed kinetics variations. Both (001) and (010) facets are called "high-energy" or "reactive" ones, and they show interesting activity in catalysis and photocatalysis. 33,34 The studies on single crystal electrodes confirmed that the (001) face had more negative flatband potential than the (101) face.³² Studies performed using luminescent measurements also showed that the surface states which serve as traps for electrons and holes has a different distribution profile in these films respect to small TiO₂ particles.³³

Morphological parameters, which can affect kinetics, can generally be summarized as the crystalline phase, surface energy, and dye loading, electron—hole distance for electron transfer, electrochemical shifts in the energy levels, and mobility of electrons in the TiO₂ conduction band. These

parameters are not necessarily independent; they could influence each other.

Having multiple injected electrons in the vicinity of the oxidized dye molecules into 400 nm TiO₂ particles gives rise to multiple back-transfer channels and an accelerated backreaction. The volume of 400 nm particles is 8000 times that of 20 nm particles. If one electron is injected per 20 nm particles under this experimental condition, a drastically larger number is expected to be injected per 200 nm particles. In addition to the number of electrons, the difference in electron diffusion (that could be faster in larger particles due to fewer particle boundaries) can add to the picture and explain the faster recombination. Large 400 nm particles used in highly efficient devices and in this study have an angular and cubic horned structure²⁶ as well as different crystalline facets rather than small particles, which then leads to an electrochemical shift of the TiO₂ conduction band and variations in dye loading behavior. In our control studies, X-ray diffraction measurements revealed that the crystalline size in the direction of (001) for small particles was estimated to be 21 nm using the Debye-Scherrer equation, which is almost equal to the size of the particles; this indicated that the most abundant crystalline phase is (101). In the case of 400 nm particles, the crystalline size for the (101) direction was only 130 nm, which was much smaller than the particle size and indicated that the particles were polycrystalline. 19 Therefore, different trap state distributions and anchoring geometries on 101 and 001 planes could also be contributing factors.

A previous theoretical study found that the TiO₂ crystallographic facet may affect the electron injection process,³⁶ and our previous ultrafast femtosecond transient absorption study of the DSC anode also showed that the electron injection pattern and early carrier dynamics in the picosecond time domain are considerably different in small 20 nm particles than those in 400 nm particles (double-layer film).¹⁹ Our current funding supports the femtosecond time-domain measurements.

It has been previously shown that the thickness of the two TiO₂ transparent and scattering layers plays a vital role in DSC device performance. Typically, a thickness of 5 + 5 or 8 + 5 for transparent and top scattering layer is used depending on the dye extinction coefficient (Ru-based with lower extinction or organic dyes with higher extinction) and the electrolyte characteristics (volatile and nonvolatile iodide-based or cobalt-based electrolytes). 27,37,38 Increasing the film thickness can increase the light harvesting efficiency, while the increase in microscopic surface area may result in increased backrecombinations. Therefore, the thicknesses were optimized²⁵ by measuring the device performance, namely photocurrent density (I_{sc}) and open-circuit voltage (V_{oc}) , and using transient photovoltage and transient photocurrent with typical time resolution of microseconds to monitor the lifetime electron back-recombination. The transient diffuse reflectance spectroscopy with nanosecond time resolution provides the possibility of optically monitoring the back-recombination and dye regeneration processes in situ.

CONCLUSIONS

We demonstrated an enhanced optical scheme for effective nanosecond time-resolved measurements of diffuse reflectance on opaque structures at low excitation powers. Because of the diffuse reflectance spectroscopy technique, we were able to monitor the kinetics of electron back-transfer in various opaque dye-sensitized ${\rm TiO_2}$ films and complete high-efficiency

DSCs. We found that the kinetics of electron back-transfer and recombination with the oxidized dye molecule is markedly affected by the morphology of the TiO2 film. Morphological parameters such as trap state distribution have a noticeable effect on the dynamics of electron back-recombination with oxidized dye molecules. In contrast to the electron backrecombination process, we did not observe such a pronounced difference in regeneration kinetics, which can be explained by this process being dependent on the differences in the dyes' highest occupied molecular orbital levels and electrolyte redox potentials. The reported nanosecond diffuse reflectance spectroscopy studies of DSC-based devices are notable in two aspects. First, they illustrated how the kinetics of electron back-recombination are different in functional devices than in experimental model systems. Second, they provide a toolbox that is applicable to noninvasive in-situ spectroscopy of opaque systems, including other types of solar cells.

ASSOCIATED CONTENT

Supporting Information

The Supporting Information is available free of charge at https://pubs.acs.org/doi/10.1021/acs.jpcc.3c05382.

I–V curve of a DSC device made with double-layer film, Z907 dye, and Z946 electrolyte; variation of Kubelka-Munk function F(R) over dye concentration at various wavelengths for dye-sensitized TiO2 double-layer-based photoanode; evolution of the absorbance spectrum of DSC samples based on Z907 sensitizer on transparent layer made of 20 nm particles at different concentrations of sensitizer; dye desorption experiment for variation of dye surface concentration on photoanodes made of transparent film and double-layer film; parameters of the exponential function fit to the signals of the nanosecond diffuse reflectance measurements on a Z907 dyesensitized photoanode made of transparent, doublelayer, and scattering films; excitation power dependence kinetics of electron back-recombination with oxidized dye molecules measured on a Z907 dye-sensitized transparent TiO₂ film made of 20 nm particles; transient diffuse reflectance measurements treated with the Kubelka-Munk function at different pulse excitation intensities on opaque photoanodes; dependence of transient KM function over changing the pulse excitation intensity; comparison of nanosecond diffuse reflectance and transmission-based laser flash photolysis measurements (PDF)

AUTHOR INFORMATION

Corresponding Author

Elham Ghadiri — Department of Chemistry and Center for Functional Materials, Wake Forest University, Winston-Salem, North Carolina 27109, United States; orcid.org/0000-0003-3406-7249; Email: ghadire@wfu.edu

Author

Jacques-E. Moser — Photochemical Dynamics Group, Institute of Chemical Sciences and Engineering (ISIC), École Polytechnique Fédérale de Lausanne (EPFL), 1015 Lausanne, Switzerland; orcid.org/0000-0003-0747-4666

Complete contact information is available at: https://pubs.acs.org/10.1021/acs.jpcc.3c05382

Notes

The authors declare no competing financial interest.

ACKNOWLEDGMENTS

We thank S. M. Zakeeruddin for providing the dye solutions and redox-active electrolytes. This work has been partially supported by National Science Foundation (NSF) through Grant 2239539.

REFERENCES

- (1) Nanosecond Laser Flash Photolysis an overview | ScienceDirect Topics. https://www.sciencedirect.com/topics/chemistry/nanosecond-laser-flash-photolysis (accessed 2023-06-27).
- (2) Teuscher, J.; Marchioro, A.; Andrès, J.; Roch, L. M.; Xu, M.; Zakeeruddin, S. M.; Wang, P.; Grätzel, M.; Moser, J.-E. Kinetics of the Regeneration by Iodide of Dye Sensitizers Adsorbed on Mesoporous Titania. *J. Phys. Chem. C* **2014**, *118* (30), 17108–17115.
- (3) Abbruzzetti, S.; Bruno, S.; Faggiano, S.; Grandi, E.; Mozzarelli, A.; Viappiani, C. Time-Resolved Methods in Biophysics. 2. Monitoring Haem Proteins at Work with Nanosecond Laser Flash Photolysis. *Photochem. Photobiol. Sci.* **2006**, *5* (12), 1109–1120.
- (4) Moser, J.-E. Dynamics of Interfacial and Surface Electron Transfer Processes. In *Dye-Sensitized Solar Cells*, 1st ed.; EPFL Press: 2010; pp 423–476.
- (5) Vulley, V. I.; Jones, G., II Nanosecond Laser Flash Photolysis: Dealing with Dynamic-Range and Response-Time Limitations of the Detection System. *J. Appl. Sci.* **2005**, *5* (3), 517–526.
- (6) Guenther, B. D.; Steel, D. Encyclopedia of Modern Optics; Academic Press: 2018.
- (7) Kessler, R. W.; Wilkinson, F. Diffuse Reflectance Triplet-Triplet Absorption Spectroscopy of Aromatic Hydrocarbons Chemisorbed on 7-Alumina. *J. Chem. SOC Faraday Trans I* **1981**, 77, 309–320.
- (8) Kessler, R. W.; Krabichler, G.; Uhl, S.; Oelkrug, D.; Hagan, W. P.; Hyslop, J.; Wilkinson, F. Transient Decay Following Pulse Excitation of Diffuse Scattering Samples. *Opt. Acta Int. J. Opt.* **1983**, 30 (8), 1099–1111.
- (9) Kortüm, G. Reflectance Spectroscopy; Principles and Applications; Springer: Heidelberg, 1969.
- (10) Wilkinson, F.; Willsher, C. J.; Uhl, S.; Honnen, W.; Oelkrug, D. Optical Detection of a Photoinduced Thermal Transient in Titanium Dioxide Powder by Diffuse Reflectance Laser Flash Photolysis. *J. Photochem.* **1986**, 33 (3), 273–278.
- (11) Litman, Y.; Voss, M. G.; Rodríguez, H. B.; San Román, E. Effect of Concentration on the Formation of Rose Bengal Triplet State on Microcrystalline Cellulose: A Combined Laser-Induced Optoacoustic Spectroscopy, Diffuse Reflectance Flash Photolysis, and Luminescence Study. J. Phys. Chem. A 2014, 118 (45), 10531–10537.
- (12) Schneider, J.; Nikitin, K.; Dillert, R.; Bahnemann, D. W. Laser-Flash-Photolysis-Spectroscopy: A Nondestructive Method? *Faraday Discuss.* **2017**, *197*, 505–516.
- (13) Stopper, K.; Dohrmann, J. K. Laser-Induced Reactions on 2.4-Nm Colloidal TiO₂ Particles in Aqueous Solution: A Study by Time-Resolved Optoacoustic Calorimetry. Z. Phys. Chem. **2000**, 214, 555.
- (14) Grätzel, M. Photoelectrochemical Cells. *Nature* **2001**, 414, 338-344.
- (15) Hagfeldt, A.; Boschloo, G.; Sun, L.; Kloo, L.; Pettersson, H. Dye-Sensitized Solar Cells. *Chem. Rev.* 2010, 110 (11), 6595–6663.
- (16) Hardin, B. E.; Snaith, H. J.; McGehee, M. D. The Renaissance of Dye-Sensitized Solar Cells. *Nat. Photonics* **2012**, *6* (3), 162–169.
- (17) Ardo, S.; Meyer, G. J. Photodriven Heterogeneous Charge Transfer with Transition-Metal Compounds Anchored to TiO ₂ Semiconductor Surfaces. *Chem. Soc. Rev.* **2009**, *38* (1), 115–164.
- (18) Bauer, C.; Banerji, N.; Wielopolski, M.; De Jonghe, J.; Ghadiri, E.; Marchioro, A.; Punzi, A.; Brauer, J. C.; Teuscher, J.; Moser, J.-E. Dynamics and Mechanisms of Interfacial Photoinduced Electron Transfer Processes of Third Generation Photovoltaics and Photocatalysis. *CHIMIA* **2011**, *65* (9), 704–704.

- (19) Ghadiri, E.; Zakeeruddin, S. M.; Hagfeldt, A.; Grätzel, M.; Moser, J.-E. Ultrafast Charge Separation Dynamics in Opaque, Operational Dye-Sensitized Solar Cells Revealed by Femtosecond Diffuse Reflectance Spectroscopy. *Sci. Rep.* **2016**, *6* (1), 24465.
- (20) McNeil, L. E.; Hanuska, A. R.; French, R. H. Orientation Dependence in Near-Field Scattering from TiO₂ Particles. *Appl. Opt.* **2001**, *40* (22), 3726–3736.
- (21) McNeil, L. E.; French, R. H. Multiple Scattering from Rutile TiO₂ Particles. *Acta Mater.* **2000**, *48* (18–19), 4571–4576.
- (22) Mudgett, P. S.; Richards, L. W. Multiple Scattering Calculations for Technology. *Appl. Opt.* **1971**, *10* (7), 1485–1502.
- (23) Sasanpour, P.; Mohammadpour, R. Theoretical Calculation of Scattering Efficiency of Isotropic and Anisotropic Scattering Particles Employed in Nanostructured Solar Cells. *J. Opt.* **2014**, *16* (5), 055703
- (24) Son, M.-K.; Seo, H.; Kim, S.-K.; Hong, N.-Y.; Kim, B.-M.; Park, S.; Prabakar, K.; Kim, H.-J. Analysis on the Light-Scattering Effect in Dye-Sensitized Solar Cell According to the TiO ₂ Structural Differences. *Int. J. Photoenergy* **2012**, *2012*, 1–8.
- (25) Ito, S.; Murakami, T. N.; Comte, P.; Liska, P.; Grätzel, C.; Nazeeruddin, M. K.; Grätzel, M. Fabrication of Thin Film Dye Sensitized Solar Cells with Solar to Electric Power Conversion Efficiency over 10%. *Thin Solid Films* **2008**, *516* (14), 4613–4619.
- (26) Ito, S.; Nazeeruddin, M. K.; Zakeeruddin, S. M.; Péchy, P.; Comte, P.; Grätzel, M.; Mizuno, T.; Tanaka, A.; Koyanagi, T. Study of Dye-Sensitized Solar Cells by Scanning Electron Micrograph Observation and Thickness Optimization of Porous TiO 2 Electrodes. *Int. J. Photoenergy* **2009**, 2009, 1–8.
- (27) Yum, J.-H.; Baranoff, E.; Kessler, F.; Moehl, T.; Ahmad, S.; Bessho, T.; Marchioro, A.; Ghadiri, E.; Moser, J.-E.; Yi, C.; et al. A Cobalt Complex Redox Shuttle for Dye-Sensitized Solar Cells with High Open-Circuit Potentials. *Nat. Commun.* **2012**, 3 (1), 631.
- (28) Schuster, A. Radiation Through a Foggy Atmosphere. Astrophys. J. 1905, 21, 1.
- (29) Enea, O.; Moser, J.; Grätzel, M. Achievement of Incident Photon to Electric Current Conversion Yields Exceeding 80% in the Spectral Sensitization of Titanium Dioxide by Coumarin. *J. Electroanal. Chem. Interfacial Electrochem.* 1989, 259 (1), 59–65.
- (30) Ghadiri, E.; Taghavinia, N.; Zakeeruddin, S. M.; Grätzel, M.; Moser, J.-E. Enhanced Electron Collection Efficiency in Dye-Sensitized Solar Cells Based on Nanostructured TiO₂ Hollow Fibers. *Nano Lett.* **2010**, *10* (5), 1632–1638.
- (31) Ghadiri, E.; Taghavinia, N.; Aghabozorg, H. R.; Zad, A. I. TiO₂ Nanotubular Fibers Sensitized with CdS Nanoparticles. *Eur. Phys. J. Appl. Phys.* **2010**, 50 (2), 20601.
- (32) Laskova, B.; Zukalova, M.; Kavan, L.; Chou, A.; Liska, P.; Wei, Z.; Bin, L.; Kubat, P.; Ghadiri, E.; Moser, J. E.; et al. Voltage Enhancement in Dye-Sensitized Solar Cell Using (001)-Oriented Anatase TiO₂ Nanosheets. *J. Solid State Electrochem.* **2012**, *16* (9), 2993–3001.
- (33) Martsinovich, N.; Troisi, A. How TiO₂ Crystallographic Surfaces Influence Charge Injection Rates from a Chemisorbed Dye Sensitiser. *Phys. Chem. Chem. Phys.* **2012**, *14* (38), 13392.
- (34) Pan, J.; Liu, G.; Lu, G. Q. M.; Cheng, H.-M. On the True Photoreactivity Order of {001}, {010}, and {101} Facets of Anatase TiO₂ Crystals. *Angew. Chem., Int. Ed.* **2011**, 50 (9), 2133–2137.
- (35) Rex, R. E.; Knorr, F. J.; McHale, J. L. Surface Traps of TiO ₂ Nanosheets and Nanoparticles as Illuminated by Spectroelectrochemical Photoluminescence. *J. Phys. Chem. C* **2014**, *118* (30), 16831–16841.
- (36) Martsinovich, N.; Troisi, A. How TiO₂ Crystallographic Surfaces Influence Charge Injection Rates from a Chemisorbed Dye Sensitiser. *Phys. Chem. Chem. Phys.* **2012**, *14* (38), 13392–13401.
- (37) Chen, C.-Y.; Wang, M.; Li, J.-Y.; Pootrakulchote, N.; Alibabaei, L.; Ngoc-le, C.; Decoppet, J.-D.; Tsai, J.-H.; Grätzel, C.; Wu, C.-G.; et al. Highly Efficient Light-Harvesting Ruthenium Sensitizer for Thin-Film Dye-Sensitized Solar Cells. *ACS Nano* **2009**, 3 (10), 3103–3109.

- (38) Yum, J.-H.; Holcombe, T. W.; Kim, Y.; Rakstys, K.; Moehl, T.; Teuscher, J.; Delcamp, J. H.; Nazeeruddin, M. K.; Grätzel, M. Blue-Coloured Highly Efficient Dye-Sensitized Solar Cells by Implementing the Diketopyrrolopyrrole Chromophore. *Sci. Rep.* **2013**, 3 (1), 2446
- (39) Luebbering, H.; Shafiee, A.; Teymur, B.; Kim, Y.; Mitzi, D. B.; Ghadiri, E. Ultrafast Microscopy and Image Segmentation of Spatially Heterogeneous Excited State and Trap Passivation in Cu2BaSnSSe3. *Cell Rep. Phys. Sci.* **2023**, *4*, 101601.
- (40) Ghadiri, E.; Shin, D.; Shafiee, A.; Warren, W. S.; Mitzi, D. B. Grain-Resolved Ultrafast Photophysics in Cu2BaSnS 4— x Sex Semiconductors Using Pump—Probe Diffuse Reflectance Spectroscopy and Microscopy. ACS Appl. Mater. Interfaces 2018, 10 (46), 39615.
- (41) DeMarco, M.; Ballard, M.; Grage, E.; Nourigheimasi, F.; Getter, L.; Shafiee, A.; Ghadiri, E. Enhanced Photochemical Activity and Ultrafast Photocarrier Dynamics in Sustainable Synthetic Melanin Nanoparticle-Based Donor—Acceptor Inkjet-Printed Molecular Junctions. *Nanoscale* **2023**, *15* (35), 14346—14364.
- (42) Ghadiri, E.; Zakeeruddin, S. M.; Hagfeldt, A.; Gratzel, M.; Moser, J.-E. Ultrafast Charge Separation Dynamics in Opaque, Operational Dye-Sensitized Solar Cells Revealed by Femtosecond Diffuse Reflectance Spectroscopy. *Sci. Rep.* **2016**, *6*, 24465 DOI: 10.1038/srep24465.